First-principles indicators of metallicity and cation off-centricity in the IV-VI rocksalt chalcogenides of divalent Ge, Sn, and Pb

U. V. Waghmare*
Jawaharlal Nehru Center for Advanced Scientific Research, Bangalore, 560 064, India

N. A. Spaldin†
Materials Department, University of California, Santa Barbara, CA 93106

H. C. Kandpal‡
Solid State and Structural Chemistry Unit, Indian Institute of Science, Bangalore, 560 012, India

Ram Seshadri§
Solid State and Structural Chemistry Unit, Indian Institute of Science, Bangalore, 560 012, India

We use first-principles density functional theory to calculate the phonon frequencies, electron localization lengths, Born effective charges, dielectric response, and conventional electronic structures of the IV-VI chalcogenide series. The goals of our work are twofold: first, to determine the detailed chemical composition of lone pairs and, second, to identify the factors that cause lone pairs to favor high- or low-symmetry environments. Our results show that the traditional picture of cation *s*-*p* mixing causing localization of the lone pair lobe is incomplete, and instead the *p* states on the anion also play an important role. In addition these compounds reveal a delicate balance between two competing instabilities—structural distortion and tendency to metallicity—leading, at the same time, to anomalously large Born effective charges as well as large dielectric constants. The magnitude of the LO-TO splitting, which depends on the relative strength of both instabilities, shows a trend consistent with the structural distortions in these compounds.

I. INTRODUCTION

Many compounds containing group IV A and V A elements with a stable valency 2 smaller than the group valency show interesting physical properties.[1,2] These include perovskite oxides with Pb^{II} on the *A* site, as well as oxides of Sn^{II}, Bi^{III}, etc. In particular, the cations in these compounds almost always occupy an off-centric position with respect to the coordination polyhedron of anions. A common aspect in these compounds is that the cations have a pair of *s* electrons in their valence shells that is often called a *lone pair*. They are structurally quite different from compounds containing cations of identical valence and similar size, but which have no lone pair.[1,2]

The activity and role of the lone pair has long been invoked for explaining the off-centering structural distortion. Starting from the early work of Sidgwick and Powell[3] and of Gillespie and Nyholm,[4] the so-called valence shell electron pair repulsion theory (VSEPR) evolved to explain and understand the geometries of molecules containing lone pair atoms. Orgel[5] invoked the mixing of *s* and *p* orbitals of cations and their polarizability to explain the structural distortions. He emphasized the generality of stereochemical effects of the lone pair and even related it to a large dielectric response. However, not all the relevant compounds (for example, of Pb^{II}) display off-centric coordination. A well-known example is PbS wherein PbS_6 octahedra are perfectly regular. This would suggest that the anion and perhaps the geometry have a role to play in whether the lone pair displays a tendency to off-centric coordination—a tendency that we shall refer to as *stereochemical activity.*

Indeed Bersuker[6] has argued that stereochemical activity is determined by a balance between the energy separation between the predominantly anion-based highest occupied orbitals and cation-based lowest unoccupied orbitals, the force constant of the mode corresponding to the distortion, and the vibronic constant, $F=\langle\psi_{anion}|(\partial V/\partial Q)_0|\psi_{cation}\rangle$. Here ψ_{anion} is the wave function of the largely anion-based highest occupied orbital, ψ_{cation} that of the largely cation-based lowest unoccupied orbital, and $(\partial V/\partial Q)_0$ the change in potential energy with distortion around the symmetric structure. In recent work, Watson and Parker[7] and Lefebvre *et al.*[8] have used electronic structure calculations to show that the anions do play an important role in the stereochemistry of PbO, the tin monochalcogenides, and the antimony chalcogenides. In addition, the effect of the lone pair on structure in Sn and Pb compounds has been visualized using electron localization functions.[9] Finally it has been implicated as playing an important role in the technologically important perovskites $PbTiO_3$ and $PbZrO_3$ and also in Bi^{III}-based compounds.[9–11]

The goals of our work in this paper are twofold. First, using the group-IV chalcogenides as a model system, we determine the detailed nature of the lone pair in distorted structures. Second, we identify which factors are important in promoting off-center distortion driven by lone-pair localization and search for a single parameter, available for the high-symmetry phase, that can be used to *predict* whether or not a particular structure will distort spontaneously. Our method of choice is density functional theory, which allows us to evaluate trends in a range of electronic and lattice dy-

TABLE I. Experimentally known structures (Ref. 1) of the IV-VI compounds. P denotes black phosphorus structure, N the rocksalt, and As a rhombohedral structure.

	S	Se	Te
Ge	P	P	As / N
Sn	P	P	N
Pb	N	N	N

namic properties, including dielectric constants and Born effective charges (BEC's), across the nine different AQ compounds with $A=$ Ge, Sn, Pb; $Q=$ S, Se, Te.

We reach two main conclusions. First, it is the stereochemical activity of the cation lone pair which is the primary driving force for structural distortion in these materials. This in turn is determined by the interaction of cation *s* and *p* states with *anion p* states; the simple traditional picture of vibronic interaction between cation *s* and *p* states is incomplete. Second, two different instabilities (the tendency to become semimetals through the closing of the gap and the structural instability) determine the properties of these nine compounds. While the BEC's are anomalously large near both of these instabilities, the splitting between the longitudinal and transverse optical phonons (LO-TO splitting) vanishes at the former and is large near the latter. The LO-TO splitting therefore reproduces the observed trends of stability, and we suggest that it is a better indicator of structural instability (and therefore more useful in designing new noncentrosymmetric compounds) than the traditional BEC.

II. EXPERIMENTAL STRUCTURES

None of the monoxides of the divalent carbon group elements Ge^{II}, Sn^{II}, and Pb^{II} crystallize in the cubic rocksalt structure. While GeO is only stable above 1273 K, SnO and PbO have a layered tetragonal structure with cations having a coordination of 4. This is notable since *all* the alkaline earth oxides MgO, CaO, SrO, and BaO are cubic rocksalts with six-coordinate cations and anions, this despite the rather large variation in size between these cations. Therefore the tendency *not* to adopt the cubic structure by certain carbon group chalcogenides cannot be explained simply from size effects. For all three cations, the rocksalt structure becomes increasingly stable as the anion is changed from O to S, Se, and then finally Te (see Table I). GeS, GeSe, SnS, and SnSe form a layered low-symmetry structure characterized by four-coordinated cations and GeTe undergoes a structural transition between 600 K and 700 K from the high-temperature rocksalt phase to a rhombohedrally distorted rocksalt structure at low temperature.[12] Table I summarizes the crystal structure data on the AQ compounds, and the experimental structures of GeS (from Ref. 13), PbTe, and GeTe are shown in Fig. 1. The tendency to be stable in the cubic rocksalt structure increases as one moves to the heavier cation-anion pairs (to bottom right).

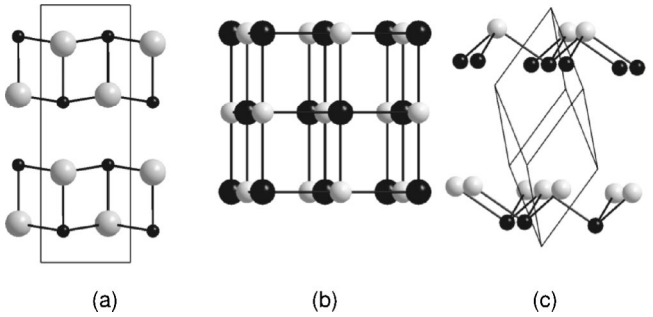

FIG. 1. Experimental structures of the IV-VI compounds. (a) is the tetragonal black phosphorus structure of GeS, (b) is the rocksalt structure of PbTe, and (c) is the polar rhombohedral low-temperature structure of GeTe. The black spheres represent the cations and the gray spheres the anions.

III. METHODS AND TECHNICAL DETAILS

In the present work, we use a combination of two first-principles density functional theory[14] (DFT) methods: the linear muffin-tin orbital (LMTO) method[15] in the atomic sphere approximation (ASA) and plane-wave pseudopotential total energy and linear response calculations.[16] The former is used to obtain partial and full densities of electronic states, crystal orbital Hamiltonian populations (COHP's) and electron localization functions (ELF's), and the latter to determine equilibrium lattice constants, TO-phonon frequencies, dielectric constant, Born effective charges, and electron localization lengths.

Our linear muffin-tin orbital ASA implementation[15] is version 47C of the Stuttgart tight-binding (TB) LMTO-ASA program.[17] A detailed description of the LMTO-ASA method, including its applications, can be found elsewhere.[18] The partitioning of space into atom-centered and empty spheres was achieved using a procedure that ensured overlap between atomic spheres did not exceed 16%. Scalar-relativistic Kohn-Sham equations within the local density approximation[19] were solved, taking all relativistic effects into account except for the spin-orbit coupling. Here 256 irreducible *k* points were used in the primitive wedge of the Brillouin zone (BZ) for the LMTO calculations. The LMTO electronic structures were analyzed by calculating COHP's and ELF's. The crystal orbital Hamiltonian population COHP (Ref. 20) is the density of states weighted by the corresponding Hamiltonian matrix element and is indicative of the strength and nature of a bonding (positive COHP) or antibonding (negative COHP) interaction. The signs we use here are the opposite of what is used in the original definition of Dronskowski and Blöchl.[20] Electron localization functions (introduced by Becke and Edgecombe) facilitate visualization of bonding and the lone pairs in real space.[21,22] The ELF provides a measure of the local influence of Pauli repulsion on the behavior of electrons and permits the mapping in real space of core, bonding, and nonbonding regions in a crystal.[22] All LMTO calculations used cell parameters obtained in our CASTEP calculations (Table II) described below.

In the plane-wave based methods, we use scalar-relativistic norm-conserving pseudopotentials optimized[23] for low plane-wave cutoffs (up to 50 Ry). The cutoff radii are

TABLE II. Calculated rocksalt unit cell volumes (Å^3) for the cubic unit cells containing four formula units.

	S	Se	Te
Ge	152.27	167.28	200.20
Sn	185.19	205.38	236.03
Pb	199.18	218.17	254.84

chosen to be close to those quoted in Ref. 24. The exchange-correlation energy functional was evaluated within the local density approximation (LDA), using the Perdew-Zunger parametrization[25] of the Ceperley-Alder[26] homogeneous electron gas data. Similar techniques have been used previously in the study of GeTe,[27] SnTe, and PbTe,[28] and related methods have been used to calculate the properties of PbS, PbSe, and PbTe.[29] Our calculations reproduce the earlier results for structural properties to within 1%. Our calculated unit cell volumes are presented in Table II. For accurate descriptions of these low-band gap materials, particularly in the calculation of phonons and dielectric properties, we sample the Brillouin zone with a $12\times12\times12$ mesh of Monkhorst-Pack k points. In the present work, total energy calculations have been performed using CASTEP 2.1 (Ref. 30) and linear response calculations with the LRESP code.[31] Both codes are based on the variational principle of density functional theory and use the conjugate gradient algorithm for direct minimization of the total energy and its second derivative.

While the calculation of dielectric constants, Born effective charges, and phonons has now become a routine application of the DFT linear response,[32] we show here that it can also be trivially used to calculate the electron localization tensor, introduced by Souza *et al.*[33] This tensor is a measure of the spread of electron Wannier functions, and its trace is equal to the gauge invariant part of[33,34]

$$\Omega=\sum_{n}^{N}\ [\langle r^2\rangle_n-\langle r\rangle_n^2],$$

where $\langle\rangle_n$ denotes the expectation value over the nth Wannier function and the sum is over the occupied bands. It is useful in the present study to probe the metallicity of a given material. Following the work of Sgiarovello *et al.*,[35] the localization tensor can be shown to be

$$\langle r_\alpha r_\beta\rangle_c=\frac{V}{N_e(2\pi)^3)}\int d\vec{k}\sum_n\ \left\langle\frac{\partial}{\partial k_\alpha}u_{n\vec{k}}\right|P\left|\frac{\partial}{\partial k_\beta}u_{n\vec{k}}\right\rangle,\quad(1)$$

where $P=1-\Sigma_n^N|u_{n\vec{k}}\rangle\langle u_{n\vec{k}}|$ is the projection operator on unoccupied states, V the volume of unit cell, and N_e the number of electrons. Here $\langle r_\alpha r_\beta\rangle_c$ indicates $\langle r_\alpha r_\beta\rangle-\langle r_\alpha\rangle\langle r_\beta\rangle$ with the average taken over all the occupied bands.

In the calculation of the dielectric constant ϵ_∞, using the DFT linear response to electric field perturbation $H_E^{(1)}$, the functions

$$H_E^{(1)}|u_{n\vec{k}}\rangle=P\left|\frac{\partial}{\partial k_\beta}u_{n\vec{k}}\right\rangle\quad(2)$$

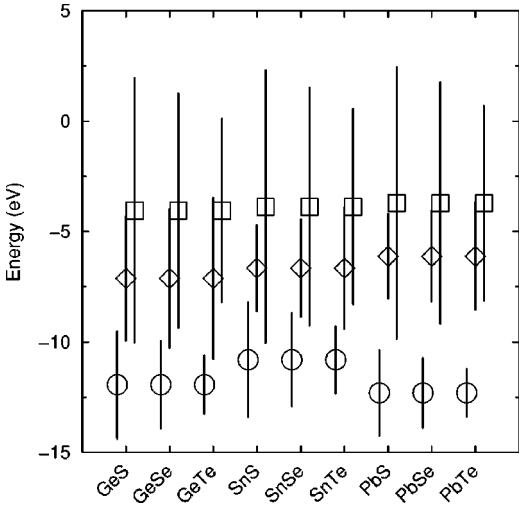

FIG. 2. Atomic orbital energies (points) and intrinsic widths of bands (vertical lines) arising from them for the nine IV-VI chalcogenides considered here. Circles and squares denote the cation s and p bands, respectively, and diamonds denote anion p bands.

have to be determined. In fact, they are obtained by calculating the first-order linear response of Kohn-Sham wave functions to a "(d/dk)" perturbation (also known as a $\vec{k}\cdot\vec{p}$ perturbation). Thus, the localization tensor can be obtained as a by-product of DFT linear response calculations of ϵ_∞ by simply taking the inner products of the intermediate wave functions given in Eq. (2).[36]

IV. PHYSICAL PROPERTIES AND THE OFF-CENTER DISTORTION

In this section we calculate various physical properties of the high-symmetry, undistorted rocksalt structures to determine whether indicators of the tendency of the structure to distort can be identified in the high-symmetry phase. The choice of physical properties is motivated by earlier studies of structural instabilities,[37] and Orgel's speculation that the polarizability or dielectric constant should be large.[5] Thus, we consider primarily those linear compliances that are a measure of coupling between phonons (lattice instability being a special case) and electric fields.

A. Band gaps

There are no notable trends in the band gaps [for example, $E_g(\mathrm{PbS})>E_g(\mathrm{PbTe})>E_g(\mathrm{PbSe})$], and in fact earlier theoretical work[29] showed that this is a result of the fine balance between the relative atomic energy levels and the strong cation-s–anion-p interactions. In Fig. 2, we show atomic orbital energies and corresponding *intrinsic* bandwidths of the ions with lattice constants of the nine chalcogenide compounds. The term energies which are symbols in the plot were obtained from atomic, scalar-relativistic calculations. For the bandwidths, which are indicated by vertical lines, self-consistent DFT calculations were performed for the carbon group atoms (Ge, Sn, Pb) and the chalcogenide atoms (S, Se, Te) in the fcc structure (rocksalt sublattice) with lat-

TABLE III. Calculated TO phonon frequencies ω (cm^{-1}) and TO force constants K (eV/Å^2) of IV-VI compounds.

		S	Se	Te
Ge	ω	110 I	90 I	97 I
	K	−2.0	−2.26	−3.2
Sn	ω	14	15 I	27
	K	0.04	−0.06	0.17
Pb	ω	111	69	52
	K	2.54	2.04	1.58

tice constants equal to the corresponding AQ compound in the rocksalt structure. These bandwidths arise therefore as a result of the crystal but in the absence of the cation-anion interaction. We point out from this figure that there is a small overlap between cation s and cation p bands for GeS, SnS, and SnSe. For GeSe, while there is no overlap, separation between the two bands is quite small. Based on Orgel's argument of cation s-p mixing, this already hints that these compounds are very likely to be unstable in the high-symmetry rocksalt structure. Note also that the p bands of the anions have decreasing overlap with the s bands of the cations as the cation or anion becomes heavier, although their overlap with the p bands of the cations is significant in *all* the compounds.

B. TO phonons

Information about phonons in the high-symmetry phase forms the foundation in modeling structural phase transitions in various materials.[38] In particular, one focuses on the lowest-energy structural distortions which span the unstable phonons characterized by imaginary phonon frequencies. We calculated the TO phonon frequencies of the IV-VI compounds, summarized in Table III along with the TO eigenvalue of the force constant matrix (which is the second derivative of energy with respect to atomic displacements). These results were obtained at the theoretical lattice constant and therefore should not agree quantitatively with experimental values due to the sensitivity of phonon frequencies to volume.[27] To benchmark our methods, we also calculated phonon frequencies at the experimental volume(s) for the compounds for which data are available and obtained results (not reported here), in good agreement with experiment.[39]

The TO phonons of the three Pb compounds and SnTe are stable, consistent with the lack of experimentally observed distortion, reported in Table I. For Sn compounds, the TO phonon is marginally stable for SnS and unstable for SnSe. For all three Ge compounds, TO phonons are unstable. At first sight, the sign and magnitude of the TO phonon frequency might appear to be a good indicator of the extent of structural instability. In fact, the frequencies *do* increase as one goes down the column; however, there is no trend along rows. While the force constant K shows a trend along rows, it is the opposite of what one would expect from the trend in stability of the cubic structure. While these results are consistent with the experimental structures listed in Table I, they do not help in understanding the relative stabilities of these compounds or in predicting trends in new structures.

TABLE IV. Calculated Born effective charges in IV-VI compounds.

	S	Se	Te
Ge	5.98	7.41	10.8
Sn	5.75	6.52	8.26
Pb	4.48	5.05	6.16

C. Born effective charges

The concept of Born effective charge is often interpreted as an indicator of ferroelectric or structural instability, and previous work on ferroelectric perovskites[37,40–43] has clearly shown that BEC's tend to be far larger than the nominal ionic charges in most ferroelectric materials. The formal definition of a BEC ($Z^*_{j,\alpha\beta}$) is the atomic position derivative of the polarization $\mathbf{P}$ at zero macroscopic electric field:

$$Z^*_{j,\alpha\beta}=\left.\frac{\partial P_\alpha}{\partial u_{j,\beta}}\right|_{\mathcal{E}=0}, \tag{3}$$

where j runs over the atoms, and α and β are Cartesian indices. Alternatively, the BEC can be defined as the linear-order coefficient between the electric field $\boldsymbol{\mathcal{E}}$ and the force $\mathbf{F}_j$ which the field exerts on ion j:

$$Z^*_{j,\alpha\beta}=\left.\frac{\partial F_{j,\alpha}}{\partial \mathcal{E}_\beta}\right|_{u=0}. \tag{4}$$

Here the derivative is calculated at zero atomic displacement or as the mixed second derivative of the total energy with respect to both electric field and atomic displacement:

$$Z^*_{j,\alpha\beta}=\left.\frac{\partial^2 E_{TOT}}{\partial \mathcal{E}_\beta \partial u_{j,\alpha}}\right|_{\mathcal{E}=0,u=0}. \tag{5}$$

A large BEC indicates that the force acting on a given ion due to the electric field generated by the atomic displacements is large even if the field is small, thus favoring the tendency towards a polarized ground state.

In Table IV we list our calculated BEC's for the cations in the IV-VI compounds, all of which have a nominal ionic charge of 2+. Since the compounds are all binary, the anion BEC's are equal to those of the cations but with opposite sign. The BEC's of all the nine compounds are quite anomalous (in fact, they deviate more from the nominal ionic charges than is typical in perovskite oxide ferroelectrics).

Two clear trends can be seen from the table: first, that the Born effective charge increases *up* the columns—that is, as the cation becomes lighter—and second, that it increases *along* the rows, as the anion becomes heavier.

The increase in Born effective charge from Pb to Sn to Ge for the same anion is consistent with the increased tendency to distortion for the lighter cations. However, the increase in BEC for heavier anions is *opposite* to the increasing ten-

TABLE V. Calculated dielectric constants ϵ^{∞} and localization lengths squared l^2 in IV-VI compounds.

		S	Se	Te
Ge	ϵ^{∞}	36.0	67.0	155.0
	l^2 (Å^2)	0.90	1.25	2.02
Sn	ϵ^{∞}	62.0	100.	93.0
	l^2 (Å^2)	1.06	1.41	1.78
Pb	ϵ^{∞}	19.0	26.0	34.0
	l^2 (Å^2)	0.81	1.02	1.33

dency to distort. Moreover, the BEC's for all nine compounds including the stable ones are anomalous (e.g., for PbTe, the BEC is 6.16). Therefore an anomalous BEC alone is clearly an insufficient indicator of a tendency to undergo ferroelectric distortion.

To understand the inadequacy of the BEC as an indicator of off-center distortion, it is helpful to rewrite the expression for the BEC using its nonvariational forms[32] as

$$Z^*_{j,\alpha\beta}=\sum_{kn}\left\langle\frac{\partial\psi_{kn}}{\partial\mathcal{E}_\beta}\middle|\frac{\partial V_{ext}}{\partial n_{j,\beta}}\middle|\psi_{kn}\right\rangle=\sum_{kn}\left\langle\frac{\partial\psi_{kn}}{\partial u_{j,\beta}}\middle|\frac{\partial V_{ext}}{\partial\mathcal{E}_\beta}\middle|\psi_{kn}\right\rangle, \tag{6}$$

where ψ_{kn} are the Kohn-Sham wave functions with Bloch vector k and band index n. It is now clear that an anomalously large BEC can occur if *either* the response to atomic displacement perturbation ($\partial\psi/\partial u_{j,\beta}$) is large, indicating a large stabilization in energy for small atomic displacements and a tendency to ferroelectric distortion, *or* if response to electric field perturbation ($\partial\psi/\partial\mathcal{E}_\beta$) is large. The latter indicates sensitivity of the wave functions to an electric field, a condition which increases with increased metallicity (or equivalently decreased ionicity) in a material. In fact the increase in BEC from S → Se → Te for the same cation is the result of such an increase in metallicity.

D. Dielectric constant and localization length

Following up on the prediction made by Orgel[5] regarding the correlation between large dielectric response and stereochemical activity of lone pairs, we study here the dielectric constants of the IV-VI compounds. Since the TO modes in some of these compounds are unstable in the rocksalt structure (making the dc dielectric constants undefined at 0 K), we focus on the high-frequency (electronic) dielectric constant ϵ^{∞}. The increase in metallicity is reflected in the magnitude of ϵ^{∞}, which diverges at the insulator to metal transition.

As mentioned in Sec. III, we also calculate the electron localization length l as a measure of metallicity. Note that the localization length is a ground state, measurable quantity with its relation[33,35] to conductivity through a sum rule. Both quantities ϵ^{∞} and l^2 are tabulated in Table V.

We find that the ϵ^{∞} is much larger than that of semiconductors (e.g., 11 for GaAs) or of perovskite oxides (<10). Similarly l^2 for most of the IV-VI compounds is much larger than values calculated previously for semiconductors[35] (about 0.7 Å^2). Both the dielectric constant and localization length increase systematically with increasing anion size, indicative of increased metallicity from S to Se to Te. This confirms that, indeed, the increased metallicity, rather than an increased tendency to off-center displacement, is in turn responsible for the increasingly anomalous BEC in the same direction. There is no consistent trend down the columns in either of these two quantities.

TABLE VI. Calculated longitudinal effective charges in IV-VI compounds.

	S	Se	Te
Ge	0.17	0.11	0.07
Sn	0.09	0.07	0.09
Pb	0.24	0.19	0.18

E. Longitudinal effective charge

It has been suggested recently[44] that a better indicator of proximity to a structural phase transition is the *longitudinal* effective charge $Z^L_{j,\alpha\beta}$ (LEC). The longitudinal effective charge is similar to the Born effective charge, but with $\mathcal{E}$ replaced by the external electric field $\mathcal{E}^{ex}$:

$$Z^L_{j,\alpha\beta}=\frac{\delta F_{j,\alpha}}{\delta\mathcal{E}^{ex}_\beta}=\sum_\gamma Z^*_{j,\alpha\gamma}\epsilon^{\infty\,-1}_{\gamma\beta}, \tag{7}$$

where $\epsilon^{\infty}_{\gamma\beta}$ is the optical dielectric tensor. Thus the LE'C incorporates the fact that, if the optical dielectric response is large, then large screening fields exist that can counteract a tendency to polarization.

The LEC's are tabulated in Table VI. The LEC's do indeed decrease from S to Se to Te, consistent with the observed reduced tendency to distortion. However, the increase from Pb to Sn to Ge that we saw in the BEC's and which is required to indicate increased distortion in compounds of the lighter cations does not persist in the LEC's. Therefore we conclude that the LEC's also cannot serve as a single parameter for predicting instabilities.

F. LO-TO splitting

Due to infinite range dipolar interactions, there is a nonanalyticity in the phonon spectrum at the Γ point of insulators, reflected in the splitting $\Delta\omega$ between long-wavelength transverse and longitudinal phonon frequencies. For cubic perovskite oxides, Zhong *et al.*[37] found that a giant LO-TO splitting in the phonon spectrum is correlated with the strongest instability in the system. LO-TO splitting depends on the Born effective charges, dielectric constant ϵ^{∞} and phonon eigenvectors;[37] as such, it can be readily obtained from the results presented so far. For the rocksalt structure, there is only one TO mode and hence a single LO-TO splitting, which is isotropic due to the cubic symmetry. Our calculated LO-TO splittings are tabulated for the IV-VI compounds in Table VII.

TABLE VII. Calculated LO-TO splitting (cm^{-1}) in the phonon spectrum of IV-VI compounds.

	S	Se	Te
Ge	322	221	178
Sn	134	106	76
Pb	113	72	64

We note that the magnitudes of LO-TO splittings are in general much smaller than those of the cubic perovskite oxides (which are typically around 700 cm^{-1}). This is particularly notable for GeTe, since it undergoes a ferroelectric phase transition. However, it is not surprising as the dielectric constants ϵ^{∞} of the IV-VI compounds are much larger than those of perovskites, resulting in screening of the long-range interatomic interactions. Indeed, LO-TO splitting captures the effects of both structural and metal-nonmetal instabilities and shows trends along both rows and columns that are exactly consistent with the trends in stability: It increases towards the left of the rows and up the columns.

G. Discussion: Competing instabilities

To conclude this section, we propose that the LO-TO splitting ($\Delta\omega$) can be interpreted as an order parameter for a phase transition from a polar insulating phase to a metallic phase. First, it vanishes in the metallic phase, since the strong screening by electrons in metals makes the range of interatomic interactions finite, removing the nonanalyticity in the phonon spectrum at $k=0$. Second, a large LO-TO splitting is correlated with a strong ferroelectric (structural) instability, because Coulomb interactions are important in stabilizing ferroelectric phases. Thus, $\Delta\omega$ is seen to be indicative of a metal-insulator transition at one end of its range and of a structural instability at the other. $\Delta\omega$ increases with *either* decreasing localization length *or* decreasing TO frequency.

Our results for IV-VI compounds indicate that they are close to both a structural phase transition and an insulator to metal transition. This complicates the trends in the various properties that we explored. More precisely, we find that the trends along the rows (with anions) are driven by the vicinity to metal-insulator instability whereas those along the column are driven by the vicinity to structural instabilities. Thus, we find a clear trend in localization length along rows and in TO phonon frequencies along columns. Both trends are captured simultaneously by the LO-TO splitting. The BEC's, which correspond to ''mixed'' couplings, show a trend consistent with metallicity along rows and with structural instability along columns.

Since there are two different instabilities relevant to these compounds, finally we studied the effect of freezing in one of them (the structural instability) on the other (the metallicity). For GeTe, we distorted the crystal internally with its TO instability at the Γ point (an intersublattice displacement) and calculated the change in localization length. For a sublattice displacement of 0.18 Å (3% of the lattice constant), we found that l^2 reduced from 2.02 to 1.60 (by 20%), indicating that the two instabilities must be strongly competing. Needless to say, the electronic structure calculations showed an increase in the band gap with distortion.

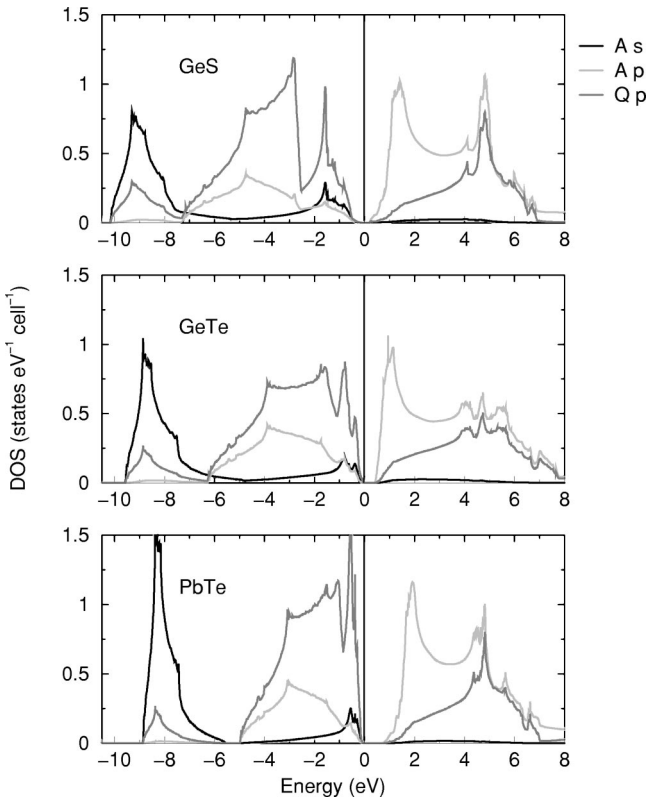

FIG. 3. Orbital-resolved LMTO densities of states for GeS, GeTe, and PbTe in the rocksalt structure. The origin on the energy axis is the top of the valence band.

V. ELECTRONIC STRUCTURE AND THE LONE PAIR

For the remainder of this work, we focus on understanding the detailed nature of the lone pair and the conditions which determine its stereochemical activity. We take GeS, GeTe, and PbTe to be representative of the nine compounds studied, with the GeS/GeTe pair allowing us to study trends in anions and GeTe/PbTe allowing us to investigate changes in behavior with the cation. We analyze the electronic structure using COHP's and visualize the lone pairs in the cubic and (hypothetical) distorted structures using ELF's.

A. Densities of states and COHP's

Figure 3 shows our calculated orbital-resolved densities of states for cubic rocksalt structure GeS, GeTe, and PbTe. The solid black line shows the cation *s* states, the light gray line the cation *p*, and the dark gray line the anion *p*. The top of the valence band is set to 0 eV. As is well known from the literature,[29] in all cases the cation *s* orbitals form the lowest-energy valence-band states forming a filled, rather narrow band, around 8 eV below the top of the valence band. The valence band is composed primarily of anion *p* states, which form a broad (around 6 eV wide) band that is somewhat hybridized with the cation *s* band. Cation *p* states dominate

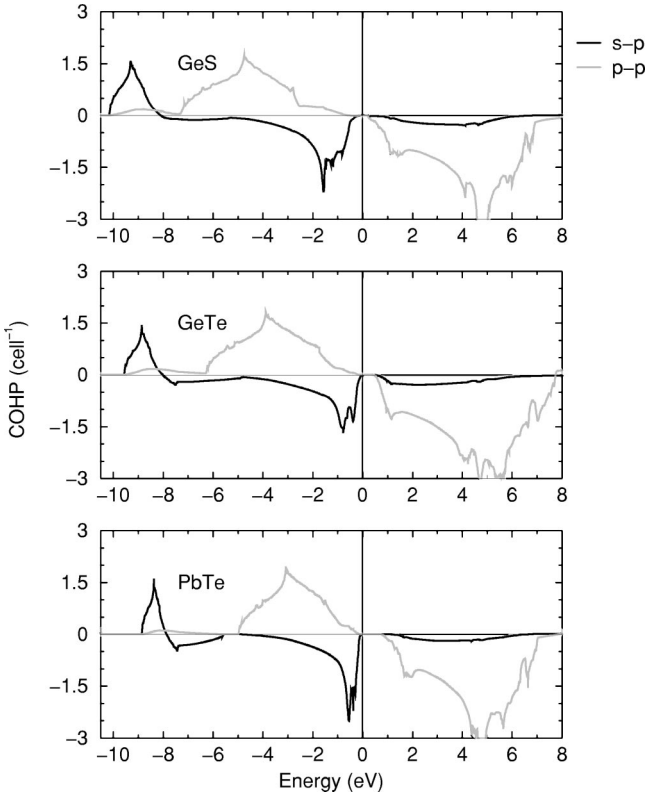

FIG. 4. COHP's per primitive unit cell for GeS, GeTe, and PbTe. The black lines correspond to cation-s–anion-p interactions and the gray lines to cation-p–anion-p interactions. Positive values of the COHP represent bonding interactions, and negative values represent antibonding interactions.

the conduction band, although there are also some occupied cation p states that overlap energetically with the anion p states. To a large extent, cation s and cation p states are well separated in energy, particularly in the structurally stable compounds such as PbTe. Indeed, PbTe even has a pseudogap centered at -5.5 eV with respect to the top of the valence band, which separates the predominantly Pb s states from the other states. In GeS, however, we note that there is a significant density of Ge s states just below the top of the valence band. A feature worthy of note is that in GeS, the Ge s states are significantly broader than those in GeTe, and these in turn are broader than Pb s states in PbTe. The bottom of the cation s states is also the deepest in GeS. Also, the system with the largest localization length of the three considered here is GeTe. This compound is the closest to metallicity and, indeed, one observes the largest fraction of cation p states in the *valence-band* region in this compound. This suggests that cation-p–anion-p covalency tends to drive the system towards metallicity.

Figure 4 shows our calculated COHP's for the same three compounds. The density of states (DOS) plots showed that, for all practical purposes, the cation s and anion p bands are filled, and the cation p states are empty. It is not surprising therefore that cation-s–anion-p interactions have both a bonding and an antibonding component *below* the top of the valence band, while cation-p–anion-p interactions are bonding below the top of the valence band and antibonding

TABLE VIII. Cation-s–anion-p, cation-p–anion-p, and total integrated COHP's (units of eV per primitive cell) for all nine compounds.

	s-p			p-p			Total		
	S	Se	Te	S	Se	Te	S	Se	Te
Ge	−1.62	−1.56	−1.86	5.22	5.22	5.40	3.60	3.66	3.54
Sn	−1.32	−1.26	−1.62	4.32	4.50	4.68	3.00	3.24	3.06
Pb	−1.56	−1.56	−1.98	4.14	4.32	4.50	2.58	2.76	2.52

above. The orbital-resolved integrated occupied COHP's reflect the energetics of the distinct bonding and antibonding interactions, with the magnitude of the integrated COHP correlating with the extent of covalency. Table VIII displays our partial and total integrated COHP's for all nine compounds. We observe that the cation-s–anion-p COHP's are indeed all negative, indicating an overall antibonding interaction. However, they do not show any simple trend along the rows or columns. In contrast, the cation-p–anion-p COHP's are all positive (indicating bonding interactions) and correlate with the localization length, supporting the link between this covalent interaction and the tendency to metallicity. The total COHP's show a trend reminiscent of the LO-TO splitting down the columns, but no clear trend along the rows.

How does the bonding situation change on distorting the rocksalt structure in a manner that allows the stereochemical activity of the lone pair to manifest itself? To answer this question, we consider GeTe in its undistorted cubic phase and in a cubic cell with a rhombohedral distortion. We obtain the distorted phase by retaining the cubic cell parameters, but displacing the Ge atom in the 111 direction by 2% in crystallographic coordinates. In other words, we retain Te at (0.5, 0.5, 0.5) and move Ge to (0.02, 0.02, 0.02) instead of keeping it at the origin. We call this the rhombohedral structure. In this structure, Ge has three nearest neighbors and three far ones, much like in the real crystal structure. Figure 5 displays the changes in calculated Ge-s–Te-p and Ge-p–Te-p COHP's on performing such a distortion. The black lines correspond to the cubic structure and the gray lines to the distorted structure. From Fig. 5, it is clear that the largest changes are in the Ge-p–Te-p COHP.

B. Electron localization functions

Figure 6 shows the calculated valence electron localization functions for GeS, GeTe, and PbTe in both cubic rocksalt and rhombohedrally distorted (as described in the previous section) structures. Following Silvi and Savin,[22] the ELF is defined as

$$\mathrm{ELF}=[1+(D/D_h)^2]^{-1},$$

where

$$D=\frac{1}{2}\sum_i |\nabla\phi_i|^2-\frac{1}{8}\frac{|\nabla\rho|^2}{\rho}, \quad D_h=\frac{3}{10}(3\pi^2)^{5/3}\rho^{5/3}.$$

Here ρ is the electron density and ϕ_i are the Kohn-Sham wave functions. The cation is at the center of the square, with

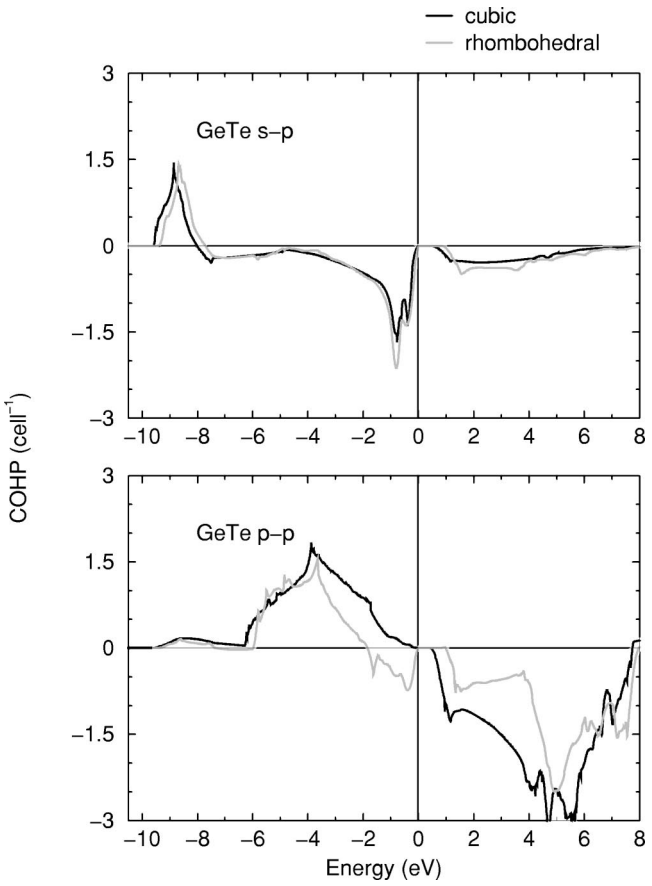

FIG. 5. COHP's of the cation-s–anion-p interaction and the cation-p–anion-p interaction for undistorted cubic and rhombohedrally distorted GeTe

.

anions in the edge centers. The white end of the scale corresponds to high localization, whereas the deep blue end indicates zero localization.

In all three cubic rocksalt cases, the s^2 lone pair is seen as a roughly spherical region of electron localization around the cation at the center of the square. (The anions, with their largely filled p shells, are also approximately spherical.) The distortion is modeled by moving the cation to the bottom left, *relative* to the anions in the picture. In all cases the formation of the localized lone pair is observed to the top right of the cation (in the space left behind).

In the systems that have distorted ground-state structures, viz., GeS and GeTe, we notice that the ELF in the lone-pair lobe (to the right of the cation) is higher than the corresponding lone-pair ELF in PbTe, which does not spontaneously distort. In addition, the lone pair has a larger spatial extent in the Ge compounds due to its increased tendency to be involved in covalent bond formation. The larger spatial extent of the lone pair seen in the ELF of GeS and GeTe when compared with PbTe is mirrored in the greater width of the cation s densities of states and the cation-s–anion-p COHP's of GeS and GeTe compared with PbTe. The combination of larger ELF and increased covalency leads to a "stronger" lone pair, which is more stereochemically active.

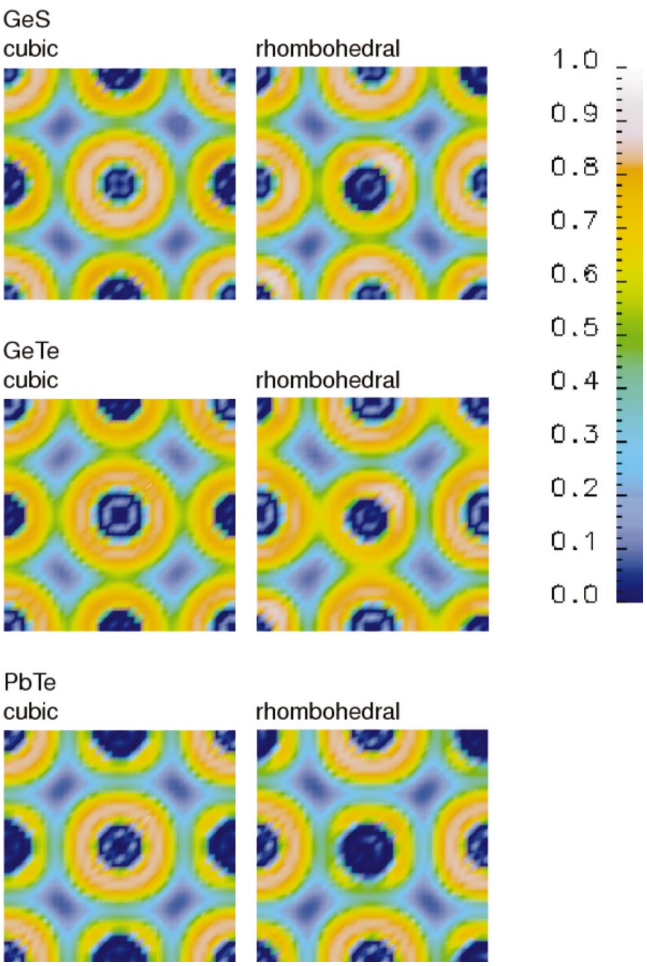

FIG. 6. (Color): Calculated valence ELF's of cubic and rhombohedrally distorted GeS, GeTe, and PbTe. Lighter colors (light gray and and white) signify regions of strong localization while colors towards dark blue signify poorly localized regions. The scale on the right of the figure indicates the color coding.

C. Discussion: Electronic structure and the lone pair

Finally, we link the physics of the two instabilities to the electronic structure and hence to the nature of the lone pair. There are three relevant electronic bands: occupied cation s (S^+), anion p (P^-), and unoccupied cation p (P^+). It was argued by Orgel,[5] and has been assumed in much of the subsequent literature, that the interaction between S^+ and P^+ bands is the primary cause of distortion. However, our results show that the mixing between S^+ and P^+ states is in fact mediated by the P^- states. This is strongest at the top of valence bands which are predominantly P^- bands (see Fig. 3). Our calculated COHP's (Fig. 4) clearly show that any S^+ and P^+ character in this energy range results from the antibonding and bonding, respectively, of S^+ and P^+ states with P^- states. A uniform structural distortion introduces P^+ states antibonding with P^- (Fig. 5) near the top of valence bands which in turn increases the mixing between S^+ and P^+. In addition, in GeS, SnS, and SnSe, there is also direct overlap between the S^+ and P^+ bands (see Fig. 2), resulting in even stronger interaction and hence structural instability.

There is an increase in anion *p* and cation *p* mixing as one goes from GeS to GeTe (see Fig. 3) correlating with increase in metallicity. Due to larger separation between S^+ and P^- bands, there is a decrease in S^+ and P^- (hence P^+) bonding when one moves from GeTe to PbTe correlating with increased structural stability. The activity of the lone pair depends on the bandwidths of and separation between all three bands. It is stronger where the mixing of S^+ and P^+ with P^- (and also indirectly S^+ with P^+) is large, where it has the stereochemical effect of stabilizing the distorted low-symmetry structures. If this mixing is over a wider range of energy (for example, GeS and GeTe), the lone pair is expected to be diffuse. For PbTe, on the other hand, S^+ character peaks in a narrow range of energy at the top of the valence band, leading to a localized lone pair, described in Sec. IV. Stability of a structural distortion depends on whether the energy gained from mixing (or bonding) between occupied and unoccupied states compensates the energy required to promote an electron to unoccupied state. Since the same P^+ states are involved in both interactions and hence instabilities, a competition results.

Thus we conclude that lone-pair lobe formation is driven primarily by covalency between cation *s* and anion *p* states with the mediation of cation *p* states rather than by on-site *s*-*p* mixing. Note that there is experimental evidence for our conclusions in extended x-ray absorption fine structure (EXAFS) measurements for Pb-doped GeTe and Pb-doped SnTe compounds. Lebedev *et al.*[45] found that Pb or Sn atoms embedded in GeTe show a *larger* off-center distortion than they do in the parent PbTe or SnTe pure compounds. Naively this might seem counterintuitive, since the smaller GeTe lattice constant should leave less space for the cation to distort. However, it is consistent with our picture of cation-*s*–anion-*p* overlap being a driving force for off-center distortion, since this is higher in the smaller lattice constant structure.

VI. SUMMARY

We have studied the structural stability of the rocksalt IV-VI chalcogenides to determine whether it correlates with TO phonons, Born effective charges, dielectric constants, electron localization length, or LO-TO splitting. The trends in structural stability are reflected fully in the trends in LO-TO splitting and partially in other properties. We identify LO-TO splitting as a single parameter, indicating the vicinity to two instabilities: metallicity and structural instability. The electronic origin of these properties is linked with the stereochemical activity of the lone pair of electrons, which in turn is driven by cation-*s*–anion-*p* hybridization.

ACKNOWLEDGMENTS

The authors thank J. Gopalakrishnan for many stimulating discussions. N.A.S.'s funding for this work was provided by the National Science Foundation, Grant No. DMR-9973076. H.C.K. and R.S. thank the Indian Council of Scientific and Industrial Research (CSIR) for support of this work.

*Electronic address: waghmare@jncasr.ac.in

†Electronic address: nicola@mrl.ucsb.edu

‡Present address: Institut für Anorganische Chemie, Universität Mainz, Duesberg Weg 10-14, Mainz D55099, Germany. Electronic address: kandpal@mail.uni-mainz.de

§Present address: Materials Department, University of California, Santa Barbara, CA 93106. Electronic address: seshadri@mrl.ucsb.edu

[1] A. F. Wells, *Structural Inorganic Chemistry*, 4th ed. (Oxford University Press, Oxford, 1974).

[2] B. G. Hyde and S. Andersson, *Inorganic Crystal Structures* (Wiley, New York, 1989).

[3] N. V. Sidgwick and H. M. Powell, Proc. R. Soc. London, Ser. A **176**, 153 (1940).

[4] R. J. Gillespie and R. S. Nyholm, Q. Rev., Chem. Soc. **11**, 339 (1957).

[5] L. E. Orgel, J. Chem. Soc. **1959**, 3815 (1959).

[6] I. B. Bersuker, *The Jahn-Teller Effect and Vibronic Interactions in Modern Chemistry* (Plenum, New York, 1984).

[7] G. W. Watson and S. C. Parker, J. Phys. Chem. B **103**, 1258 (1999); G. W. Watson, S. C. Parker, and G. Kresse, Phys. Rev. B **59**, 8481 (1999).

[8] I. Lefebvre, M. A. Szymanski, J. O. Fourcade, and J. C. Jumas, Phys. Rev. B **58**, 1896 (1998); I. Lefebvre, M. Lannoo, G. Allan, A. Ibanez, J. Fourcade, J. C. Jumas, and E. Beaurepaire, Phys. Rev. Lett. **59**, 2471 (1987).

[9] R. Seshadri, G. Baldinozzi, C. Felser, and W. Tremel, J. Mater. Chem. **9**, 2463 (1999); J.-M. Raulot, G. Baldinozzi, R. Seshadri, and P. Cortona, Solid State Sci. **4**, 467 (2002); R. Seshadri, Proc.-Indian Acad. Sci., Chem. Sci. **113**, 487 (2001).

[10] J. Gopalakrishnan, Proc.-Indian Acad. Sci., Chem. Sci. **96**, 449 (1986).

[11] R. Seshadri and N. A. Hill, Chem. Mater. **13**, 2892 (2001).

[12] J. Goldak, C. S. Barrett, D. Innes, and W. Youdelis, J. Chem. Phys. **44**, 3323 (1966); T. B. Zhukova and A. I. Zaslavskii, Sov. Phys. Crystallogr. **12**, 28 (1967); E. P. O'Reilly, J. Robertson, and M. J. Kelly, Solid State Commun. **38**, 565 (1981).

[13] G. Bissert and K. F. Hesse, Acta Crystallogr., Sect. B: Struct. Crystallogr. Cryst. Chem. **34**, 322 (1978).

[14] P. Hohenberg and W. Kohn, Phys. Rev. **136**, 864 (1964); W. Kohn and L. J. Sham, Phys. Rev. **140**, A1133 (1965).

[15] O. K. Andersen, Phys. Rev. B **12**, 3060 (1975); O. Jepsen and O. K. Andersen, Z. Phys. B: Condens. Matter **97**, 35 (1995).

[16] M. C. Payne, M. P. Teter, D. C. Allan, T. A. Arias, and J. D. Joannopoulos, Rev. Mod. Phys. **64**, 1045 (1992).

[17] R. W. Tank, O. Jepsen, A. Burkhardt, and O. K. Andersen, The Stuttgart TB-LMTO-ASA program (version 47), MPI für Festkörperforschung, Stuttgart, Germany, 1998.

[18] H. L. Skriver, *The LMTO Method* (Springer, Berlin, 1984).

[19] U. von Barth and L. Hedin, J. Phys. C **4**, 2064 (1971).

[20] R. Dronskowski and P. E. Blöchl, J. Phys. Chem. **97**, 8617 (1993); F. Boucher and R. Rousseau, Inorg. Chem. **37**, 2351 (1998); more information on the use of COHP's can be found at www.cohp.de

[21] A. D. Becke and K. E. Edgecombe, J. Chem. Phys. **92**, 5397 (1990).

[22] B. Silvi and A. Savin, Nature (London) **371**, 683 (1994).
[23] A. M. Rappe, K. M. Rabe, E. Kaxiras, and J. D. Joannopoulos, Phys. Rev. B **41**, 1227 (1990).
[24] G. B. Bachelet, D. R. Hamann, and M. Schluter, Phys. Rev. B **26**, 4199 (1982).
[25] J. P. Perdew and A. Zunger, Phys. Rev. B **23**, 5048 (1981).
[26] D. M. Ceperley and B. J. Alder, Phys. Rev. Lett. **45**, 566 (1980).
[27] K. M. Rabe and J. D. Joannopoulos, Phys. Rev. Lett. **59**, 570 (1987); Phys. Rev. B **36**, 6631 (1987).
[28] K. M. Rabe and J. D. Joannopoulos, Phys. Rev. B **32**, 2302 (1985).
[29] S.-H. Wei and A. Zunger, Phys. Rev. B **55**, 13 605 (1997).
[30] M. C. Payne, X. Weng, B. Hammer, G. Francis, I. Stich, U. Bertram, A. de Vita, J. S. Lin, A. Qteish, and V. Milman, computer code CASTEP, Cavendish Laboratory, University of Cambridge. The code has been significantly modified and optimized by U. V. Waghmare, K. M. Rabe, and N. A. Hill.
[31] U. V. Waghmare, V. Milman, and K. M. Rabe (unpublished).
[32] X. Gonze, Phys. Rev. B **55**, 10 337 (1997).
[33] I. Souza, T. Wilkens, and R. M. Martin, Phys. Rev. B **62**, 1666 (2000).
[34] N. Marzari and D. Vanderbilt, Phys. Rev. B **56**, 12 847 (1997).
[35] C. Sgiarovello, M. Peressi, and R. Resta, Phys. Rev. B **64**, 115 202 (2001).
[36] X. Gonze (private communication). Gonze's group is also using this method to calculate electron localization lengths.
[37] W. Zhong, R. D. King-Smith, and D. Vanderbilt, Phys. Rev. Lett. **72**, 3618 (1994).
[38] K. M. Rabe and U. V. Waghmare, Phys. Rev. B **52**, 13 236 (1995).
[39] R. Dalven, Phys. Rev. B **3**, 1953 (1971).
[40] Ph. Ghosez, J.-P. Michenaud, and X. Gonze, Phys. Rev. B **58**, 6224 (1998).
[41] R. Resta, M. Posternak, and A. Baldereschi, Phys. Rev. Lett. **70**, 1010 (1993).
[42] M. Posternak, R. Resta, and A. Baldereschi, Phys. Rev. B **50**, 8911 (1994).
[43] Ph. Ghosez, X. Gonze, and J.-P. Michenaud, Ferroelectrics **153**, 91 (1994).
[44] A. Filippetti and N. A. Hill, Phys. Rev. B **65**, 195120 (2002).
[45] A. I. Lebedev, I. A. Sluchinskaya, V. N. Demin, and I. H. Munro, Phys. Rev. B **55**, 14 770 (1997).